



The Effect of the Milling Vial Shape on the *In-Situ* Consolidation of a Nanocrystalline Al-Li-GNPs Nanocomposite Synthesized by Room Temperature Ball-Milling

Sara I. Ahmad and Khaled M. Youssef*

Materials Science and Technology Graduate Program, College of Arts and Sciences, Qatar University, Doha, Qatar

Several studies investigating the ball-milling of ductile face-centered cubic metals have reported a so-called *in-situ* consolidation phenomenon where the milled powder is also consolidated during the milling process. Thus, instead of refined powders or agglomerated particles, the formation of spherical bulk particles of the milled material is reported using a combination of cryomilling and room temperature milling processes. In this study, we studied the effect of the milling vial shape on the *in-situ* consolidation of a graphene nanoplatelets (GNPs) reinforced aluminum-lithium (Al-Li) matrix nanocomposite for the first time. An *in-situ* consolidated nanometric Al-Li-GNPs nanocomposite with an average grain size of 48 nm and high hardness of 1.48 GPa was attained after only 8 h of room-temperature milling. The results presented suggest that dense nanostructured composites can be prepared by *in-situ* consolidation during a one-step milling process and subsequently investigated in order to analyze their mechanical behavior. This allows for the intrinsic mechanical behavior of the synthesized material to be examined without the interference of subsequent high-temperature consolidation processes, thus avoiding unwanted structural changes such as grain growth and second phase formations.

Keywords: *in-situ* consolidation, ball-milling, graphene, aluminum, nanocomposite

OPEN ACCESS

Edited by:

Qudong Wang,
Shanghai Jiao Tong University, China

Reviewed by:

Rajkumar Kaliyamoorthy,
SSN College of Engineering, India
Shokouh Attarilar,
Shanghai Jiao Tong University, China

*Correspondence:

Khaled M. Youssef
kyoussef@qu.edu.qa

Specialty section:

This article was submitted to
Mechanics of Materials,
a section of the journal
Frontiers in Materials

Received: 28 October 2021

Accepted: 24 January 2022

Published: 23 February 2022

Citation:

Ahmad SI and Youssef KM (2022) The Effect of the Milling Vial Shape on the *In-Situ* Consolidation of a Nanocrystalline Al-Li-GNPs Nanocomposite Synthesized by Room Temperature Ball-Milling. *Front. Mater.* 9:804075. doi: 10.3389/fmats.2022.804075

1 INTRODUCTION

The synthesis of graphene reinforced aluminum (Al) matrix composites (GRAMCs) has witnessed an exponential uprise since the beginning of the last decade (Ahmad et al., 2020a), with successfully reported enhancements in Al's mechanical strength (Shin and Bae, 2015; Zhang et al., 2016), thermal conductivity (Chen and Huang, 2013; Pradhan et al., 2020), and electrical properties (Chyada et al., 2017; Wang et al., 2019). Ball-milling is the most widely used technique for the synthesis of graphene reinforced Al matrix composites, owing to its efficient exfoliation, mixing, and distribution of the graphene nanoplatelets in the metal matrices (Ahmad et al., 2020a). However, the main issue with powder metallurgy processing techniques including the ball-milling of powders, is that an indispensable powder consolidation process must follow to attain bulk materials for reliable and reproducible mechanical testing (Koch et al., 2008). The ultimate goal is to achieve the maximum theoretical density by facilitating a complete inter-particle bonding which is essentially achieved by the incorporation of both pressure and high temperature (Koch et al., 2008; El-Danaf et al., 2013).

Different consolidation techniques result in different degrees of densification and several advanced consolidation techniques have been utilized for the synthesis of graphene reinforced MMCs including hot extrusion (El-Ghazaly et al., 2017), hot pressing (Kwon et al., 2017), microwave sintering (Rajkumar and Aravindan, 2009; Ghasali et al., 2018), hot rolling (Shin et al., 2015), and spark plasma sintering (Bisht et al., 2017; Ram Prakash et al., 2021) for mechanical properties testing. However, powder consolidation is not a trivial process and requires the optimization of the process parameters to achieve maximum densification (Awotunde et al., 2019; Attarilar et al., 2021a), without causing significant coarsening of the consolidated microstructure or introducing unwanted phases (Koch et al., 2008).

Gürbüz et al. (2017) studied the effect of sintering time on the consolidation of Al-0.1 wt% graphene nanoplatelets (GNPs). They reported that the density of the green pressed composite increased up to a sintering time of 180 min, after which the density dropped. Saheb (2013) noted that the sintering temperatures significantly influenced the densification of spark plasma sintered (SPS) A2124 and A6061 alloys. Their results showed that an increase in the sintering temperature from 450 to 550°C reduced porosity dramatically and enhanced densification. Bisht et al. (2017) reported a poor sinterability of the GNPs/Al composite at higher volume fraction addition of GNPs regardless of the sintering temperature. This is attributed to the agglomeration tendency of GNPs at higher GNPs content, which reduces the contact area between the Al particles, and prevents their rearrangement during pressing.

The quality of the consolidated bulk specimens and their densification play a key role in determining the mechanical behavior during testing. Thus, failure to achieve full densification will result in early sample failure which does not necessarily represent the material's intrinsic mechanical behavior, but rather its compacted microstructure (Koch et al., 2008). This explains the discrepancies in the mechanical performance reported for the same material synthesized by various research groups and hinders the understanding and interpretation of the synthesized intrinsic mechanical performance.

In this regard, several studies investigating the ball-milling of face-centered cubic (FCC) metals have reported a so-called *in-situ* consolidation phenomenon where the milled powder is also consolidated during the milling process (SamadiKhoshkhoo et al., 2015; Hegedüs et al., 2017; Abaza et al., 2019; Ahmed et al., 2020; Ahmad et al., 2020b). Thus, instead of refined powders or agglomerated particles, the formation of relatively large spherical bulk particles of the milled material is reported using a combination of cryomilling and room temperature milling processes. It was explained that using cryomilling resulted in the formation of small spherical agglomerates with nanoscale grain sizes, while the heat generated during room temperature milling allowed for the consolidation of the already spherical agglomerates into densified spheres with smooth surfaces (Ahmad et al., 2020b). *In-situ* consolidation is of particular advantage for the synthesis of nano-crystalline materials. It eliminates the need for consecutive high-temperature compaction processes; thus avoiding any

structural changes such as grain growth and second phase formations (Koch et al., 2008). This allows for the intrinsic mechanical behavior of the synthesized material to be examined. Koch et al. reviewed the mechanical properties of ball-milled *in-situ* consolidated nanocrystalline metals (Koch et al., 2008). Zhu et al. (2003) reported the synthesis of *in-situ* consolidated Zn spheres with 5–10 mm diameters using a combination of cryomilling and room temperature milling processes. Youssef et al. utilized a similar procedure to synthesize artifact-free *in-situ* consolidated Al-Mg (Youssef et al., 2006) and Cu (Youssef et al., 2004) spheres with enhanced mechanical properties.

The ball-milling technique has been investigated vigorously in the field of graphene reinforced metal composite. The effect of the milling time on the morphology and structure of GRAMCs (Pérez-Bustamante et al., 2014a; Bastwros et al., 2014; Jiang et al., 2018), the effect of the GNPs content on the mechanical performance of GRAMCs (Ashwath and Xavier, 2014; Zhang et al., 2016; Tiwari et al., 2020), and the effect of the milling temperature on the ball-milling of GRAMCs (Li et al., 2015) have been investigated. In addition, other reports studied the effect of the milling balls' size (Zhang et al., 2016) and the effect of the milling speed (Zhang et al., 2016; Jiang et al., 2018) on the structural integrity of graphene in GRAMCs. In this paper, the effect of the ball-milling vial and its shape on the *in-situ* consolidation of a nanocrystalline Al-Li alloy reinforced with GNPs by room temperature ball-milling is investigated for the first time. For comparison, the same nanocomposite composition was milled using the conventional cylindrical milling vial under the same conditions.

2 MATERIALS AND METHODS

Al powder with a 99.97% purity purchased from Alfa Aesar was ball-milled with 2.0 at% Li granules of 99.0% purity and 1.0 wt% GNPs purchased from Sigma-Aldrich. The 2.0 at% content of Li added was based on previous studies, which showed a complete solid solubility of Li in ball-milled Al at an atomic content less than 4.0% (Ahmad et al., 2020b). Based on literature data, 1.0 wt% content of GNPs is enough to reinforce Al-based composites mechanically (Pérez-Bustamante et al., 2014a; Li et al., 2015; Tabandeh-Khorshid et al., 2016). Ball-milling was performed using a SPEX 8000 shaker mill under argon to prevent the formation of oxides during milling. No process control agents (PCA) were used as it has been proven to interfere with the *in-situ* consolidation during the milling process. Instead, the expected excessive Al welding was mitigated by the GNPs and its self-lubricating nature, which renders its presence as a PCA during milling. In addition to the conventional cylindrical milling vial, a specially designed concaved milling vial was used to investigate the effect of the milling vial shape on the *in-situ* consolidation of Al, see **Figure 1**. Both balls used for the milling and the milling vials were made from the same type of steel (Stainless steel 440C). A total of 32 milling balls were used (16 balls with 1/4" diameter and 16 balls with 5/16" diameter) with a total ball-to-powder ratio of 17:1. To maximize the sphericity of the specifically

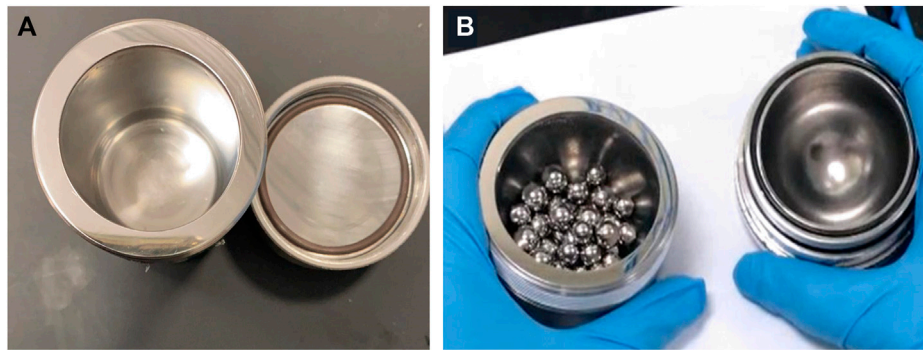


FIGURE 1 | (A) Conventional cylindrical milling vial, and **(B)** specially designed vial with a round concaved circular interior wall.

designed milling vial, the concaved milling vial consisted of two parts, see **Figure 1B**, each consisting of half a sphere with a diameter of 44.8 mm and an inner length of 32.7 mm. A portion of the mechanically milled powder was extracted after every hour of milling to observe and investigate the effect of milling and determine the optimum milling time for the Al-Li-1.0 wt% GNPs nanocomposite.

Scanning electron microscopy images (SEM) images of the as-milled particles were taken using a FEI Nova NanoSEM 450 operated at an accelerating voltage of 5 kV and a working distance of 5 mm. Structural analysis was conducted using X-ray diffraction (XRD). A PANalytical Empyrean Diffractometer with a CuK α ($\lambda = 0.1542$ nm) radiation was used at a 45 kV, 40 mA, and 25°C with scanning range from 20° to 100°, a step size of 0.013°, and a scan rate of 0.044° s⁻¹. Transmission electron microscope (TEM) analysis on the synthesized Al-Li-GNPs nanocomposites was performed using a Thermo Scientific TalosF200X TEM operating at 200 keV. The TEM samples were prepared by electrojet polishing using a Fischione double-jet electropolisher in an ethanol solution with 10% vol% perchloric acid at 0°C. A Thermo fisher scientific DXR Raman spectroscopy with a laser wavelength of 532 nm was used to examine the structural integrity of the GNPs after milling. Optical microscopy images were recorded using an OLYMPUS BX53M light microscope. Vickers microhardness measurements were carried out using a Future-Tech Microhardness Tester FM-800. The automated loading system was used with a 5 s dwell time and a 25 g load. A total of eight indentations on each sample were taken to obtain an average and calculate the standard deviation.

3 RESULTS AND DISCUSSION

The two different vials utilized in the ball-milling of the Al-Li-GNPs samples are shown in **Figure 1**. A conventional milling vial that exhibits a cylindrical-shaped inner wall with a flat top and bottom facets is shown in **Figure 1A**. The second milling vial is specially designed to induce *in-situ* consolidation during milling and exhibits a concaved circular inner wall, see **Figure 1B**.

3.1 Conventional Milling Vial

The SEM images in **Figure 2** show the morphology of the as-received Al and the Al-Li-GNPs powder extracted after different milling times. The initial as-received gas-atomized Al powder appears to be round, equiaxed particles with an average particle size of 15 μ m, see **Figure 2A**. Compared to the as-received Al (see the scale bar), it is visibly clear from the SEM images in **Figure 2** that the particle size of the Al-Li-GNPs increased significantly after milling. It is well-known that the ball-milling process can cause a considerable change to the morphology of the milled powder (Hajalilou et al., 2018) and effectively distribute and disperse the nano-reinforcement (Jiang et al., 2018). Furthermore, the ball-milling process is characterized by the competition between the cold welding of the milled powder and its fracture (Hajalilou et al., 2018; Jiang et al., 2018).

The collision force between the milling balls and the powder being milled is defined by the act of two forces, a radial compressive force, and a tangential shearing force. Powder deformation, including cold welding, flattening, and fracturing, is determined by the radial compressional force coming from the direct high energy impacts. The distribution and dispersion of the GNPs, however, is achieved by the tangential shearing force as a result of the side impacts, high-speed rotation, and the friction of the balls (Jiang et al., 2018). In order to achieve effective milling and *in-situ* consolidation of a GRAMC, enough milling time is required to achieve both matrix grain refinement and reinforcement distribution, as well as particle agglomeration and consolidation.

During the early stages of milling, the cold-welding mechanism dominated the milling process. The high ductility of Al and the heat generated during milling due to the high impact collision forces between the balls and the Al powders resulted in Al agglomeration. As a result, welding became more dominant than fracturing (Suryanarayana, 2019; Wu et al., 2018). The significant increase in the average particle size of the initial fine powders from 15 μ m to 0.45 mm after 2 h of milling, indicated that cold welding of the Al particles was clearly activated, see **Figure 2B**. During high energy ball-milling of GNPs, the high shear force and high rotation energy exerted during milling are known to induce further exfoliation and uniform distribution of the GNPs in the metal matrix (Rashad

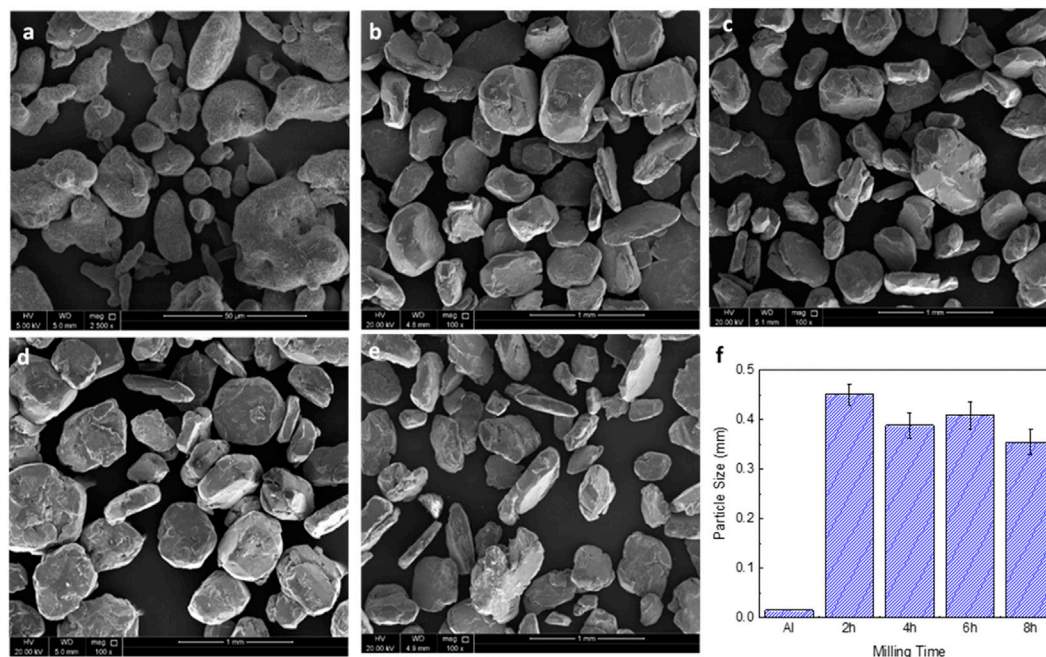


FIGURE 2 | SEM images showing the morphology of the (A) as received Al, and the as-milled Al-Li-GNPs powder after milling in the conventional milling vial for (B) 2 h, (C) 4 h, (D) 6 h, and (E) 8 h. (F) Particle size of as-milled samples vs milling time.

et al., 2015a; Yue et al., 2017; Jiang et al., 2018; Yu et al., 2019). Thus, at this stage of milling, the exfoliated and dispersed GNPs were embedded and entrapped in between the cold-welded Al-matrix particles (El-Ghazaly et al., 2017; Pérez-Bustamante et al., 2014a; Li et al., 2019). In addition, apparent flattening of the surface of the Al particles was observed. This is due to the continuous compressional deformation induced by the increased number of collisions with milling time. The average particle size decreased to 0.39 mm after 4 h of milling, indicating that the particles were hardened, deformed, and fractured at this stage (Toozandehjani et al., 2017), and then increased again to 0.41 mm after 6 h of milling, see **Figures 2C–F**. These competing events of cold welding and fracturing repeatedly continue throughout the milling period until a steady-state stage is reached (Suryanarayana, 2019). At this steady state, a homogenous microstructure was achieved as is indicated by the refined particle size, and as will be discussed in **Section 3.3**, by the homogenous composition, and the uniform grain size throughout the sample (Attarilar et al., 2021b). After 8 h of milling, the majority of the sample attained a noticeably smaller, finer, flake-like structure with an average particle size of 0.35 mm. Nonetheless, the size of the milled powders/particles after any stage of milling is larger than the size of the original Al powder. This is expected, as explained, due to the ductility of Al and the heat generated during milling, especially in the case of milling without the use of a PCA.

It is significant to note that in addition to the flat particles, the formation of spheres was observed after 8 h of milling, see **Figure 3A**. These small spheres started to form after 5 h of milling. With increased milling time, the spheres started to

agglomerate onto each other randomly to form larger irregularly shaped spheres after 8 h. With the increased milling time, deformation and fracturing, accompanied by the continuous flattening of the composite powders and a decrease in the powder size, became prominent (Li et al., 2019). Yet, at the same time, the heat generated due to the high-energy milling generated with longer milling times allowed for particles to recover and bond favoring the welding process again, which explains the presence of the agglomerated spheres (Pérez-Bustamante et al., 2014a).

In order to investigate the effect of extreme milling time on the morphology of the as-milled Al-Li-GNPs powder using the conventional milling vial, milling was continued for 40 h. It is generally known that longer milling times of ductile metals favor the welding of the milled particles (Pérez-Bustamante et al., 2014a), and can lead to the amorphization of the crystal lattice (Sakher et al., 2018). The evolution of the Al-Li-GNPs particle morphology milled in the conventional milling vial with milling time can be seen in **Figure 3**. Initially, the entire sample started agglomerating into small-sized spheres that weld together with continued milling time, see **Figure 3B**. With longer milling time, the agglomerated irregularly shaped spheres formed round-shaped spheres with uniform surfaces, see **Figure 3C**. At around 16–18 h of milling, those spheres flattened and welded on the milling balls, forming a layer due to the continuous bombardment and flattening by the high impact balls, see yellow arrow in **Figure 3D**. At this stage, the spheres took the shape of a thin curved bowl, mimicking the ball's surface. These bowl-like particles peeled off of the ball's surface after 33 h of milling; see purple arrow in **Figure 3D**. With continued milling,

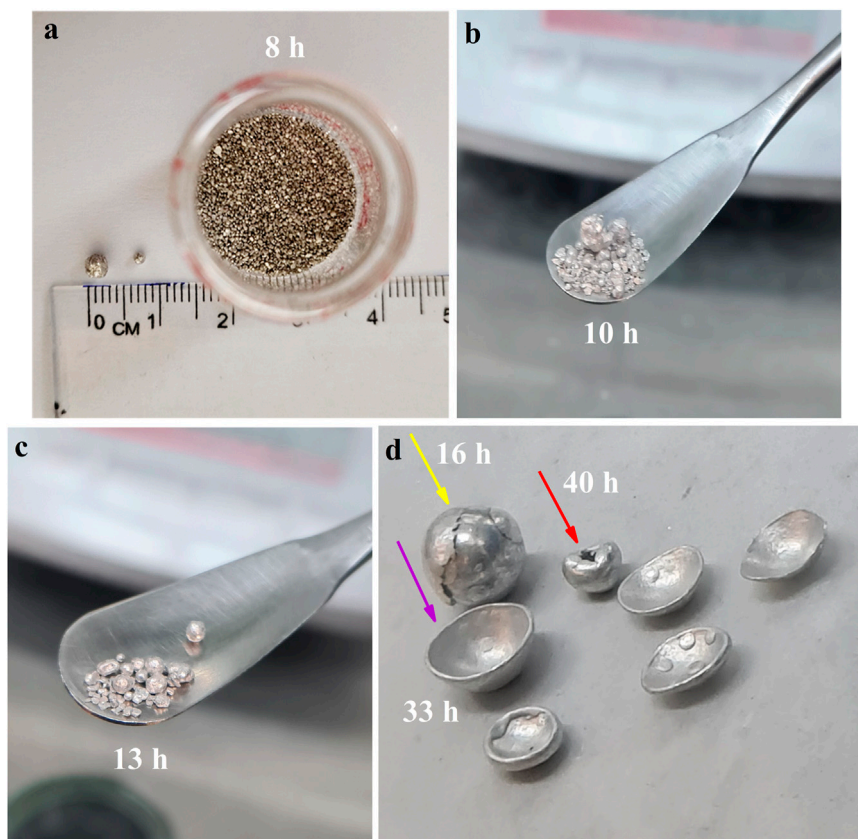


FIGURE 3 | The evolution of the Al-Li-GNPs particle morphology milled in the conventional milling vial with milling time. **(A)** 8 h, **(B)** 10 h, **(C)** 13 h, and **(D)** 16 h, 33 h, and 40 h.

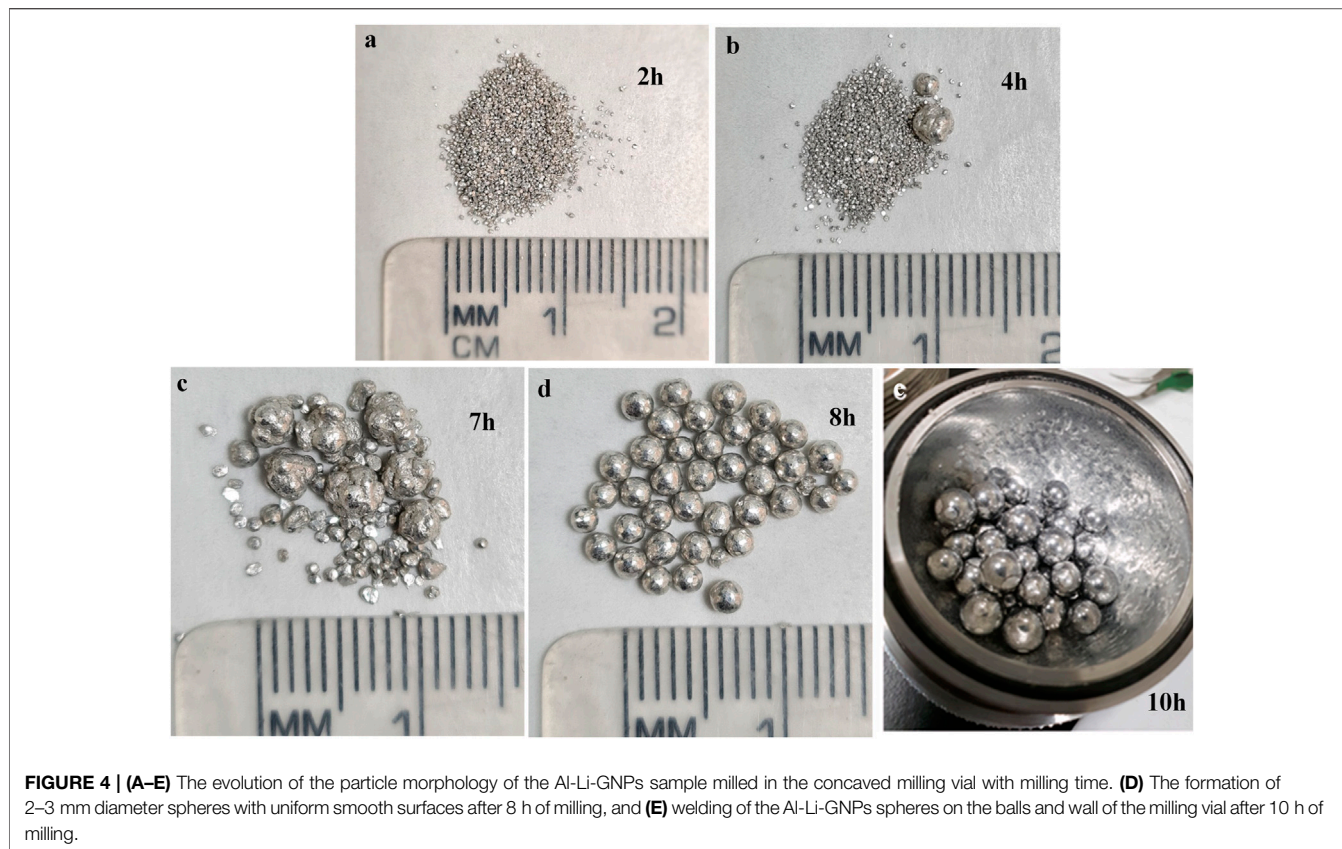
the edges of these bowl-like particles started to convolve, and after 40 h of milling, the bowl-shaped particles evolved into doughnut-like particles, see red arrow in **Figure 3D**. The synthesis of doughnut-like morphologies as a result of milling has been reported by Huang et al. (1995) and Hegedűs et al. (2017) for Cu and Pd particles, respectively. Hegedűs et al. (2017) suggested that further ball-milling resulted in closing of the hollow middle part of the particles, which led to the formation of hollow spheres.

3.2 Concaved Milling Vial

In-situ consolidation of bulk Al-Li-GNPs spheres was not achieved even with longer milling times using the conventional milling vial. A specially designed vial with circular concaved interior walls was used to investigate the effect of the milling vial shape on the *in-situ* consolidation of Al, see **Figure 1B**. The milling process was performed by utilizing the exact same composition and parameters used before in the conventional vial. Regardless of the exact mechanism for *in-situ* consolidation during milling, the cold-welding of the milled powder is a primary requirement. Al is a ductile metal, and the deformation of the particles due to the impact between the balls and the powder will be affected by where the impact is taking place.

The initial morphology observations for the sample milled in the concaved milling vial were similar to those observed for the Al-Li-GNPs sample milled in the conventional milling vial. A competition between welding and fracturing and collisions between the milling balls and milled powder resulted in the formation of flat flake-like particles. However, the small spheres started developing earlier during milling using the concaved vial, which later agglomerated onto each other randomly to form larger irregularly shaped spheres after the fourth hour, see **Figures 4A–E**.

After 6 h of milling, the particles increased in size, more spheres formed, and the tendency of agglomeration of the small spheres to form irregularly shaped spheres increased. This is attributed to the fact that at this stage, the heat generated due to high-energy milling allowed for the sample particles to recover and bond, favoring the welding process. By the end of the eighth hour, *in-situ* consolidation took place where the entire sample turned into 2–3 mm diameter spheres with uniform smooth surfaces, see **Figure 4D**. The uniformity of the particles in the entire sample after this time of milling suggested that what is known as a steady-state equilibrium stage was reached between the rate of welding and the rate of fracturing (Zhao et al., 2010; Najimi and Shahverdi, 2017). Further milling



up to 10 h resulted in the welding of a large number of spheres onto the milling balls due to the continuous high-frequency bombardment of the steel balls with the Al spheres, resulting in a lower material yield, see **Figure 4E**.

It is clear that the circular walls of the concaved vial used facilitated the formation of the initially small spheres. Thus, the *in-situ* consolidation required significantly shorter times than those reported in the literature for room temperature *in-situ* consolidation studies (Harris et al., 1993; Huang et al., 1995; Gupta et al., 2015; Hegedűs et al., 2017). The exact mechanism of *in-situ* consolidation using ball-milling is not well understood yet, as evidenced by the few publications reported in the literature (Huang et al., 1995; SamadiKhoshkhoo et al., 2015; Hegedűs et al., 2017). Nonetheless, several mechanisms have been suggested based on the morphological observations of the *in-situ* consolidated spheres.

To gain a deeper insight into the interior morphology of the spheres and the level of consolidation, several *in-situ* consolidated Al-Li-GNPs spheres milled for 8 h were covered in epoxy and polished across their diameters to investigate their densification using optical microscopy, see **Figure 5**.

All the spheres appeared to be solid bulk spheres from the outside but with different features on the inside, as observed in **Figures 5A–I**. The sphere shown in **Figure 5A** was polished slightly to reach a flat surface, where it appeared to be fully densified. At first sight, the optical image of the sphere suggested full densification due to the absence of any major cracks or

porosities. However, further polishing to reach the middle of the sphere proved that despite the *in-situ* consolidation, several curved crack-like areas appeared across the polished surface of the spheres. The nature of cracks and interfaces present is related to the cold-welding, and several formation mechanisms of the spheres have been suggested (Meyers and Taylor Aimone, 1983; Harris et al., 1993; Hegedűs et al., 2017).

From the morphological observations in **Figures 4, 5**, it is suggested that initial ball-ball and ball-vial collisions with the milled powder produced thin flakes, which later concaved to form small spheres. With milling time, the heat generated due to the high frequency and high energy collisions during milling, along with the continuous circular high energy vessel movement, and the concaved circular walls of the milling vial, facilitated the formation of either small spheres that later agglomerated together and deformed to form larger ones (sphere-to-sphere), or resulted in the formation of spherically bent particles that attached to the surfaces of the already formed spheres (flake-to-sphere). The presence of curved voids inside the spheres is attributed to the incomplete flake-to-sphere and sphere-to-sphere welding during milling. Similar *in-situ* formation mechanisms have been reported by Huang et al. (1995) and Harris et al. (1993). Other spheres polished to varying degrees, see **Figure 5**, showed different interior structures, but with a common feature where the outside areas of the spheres showed better consolidation than the inner parts of the spheres. When the initially small spheres weld together, their combined inner

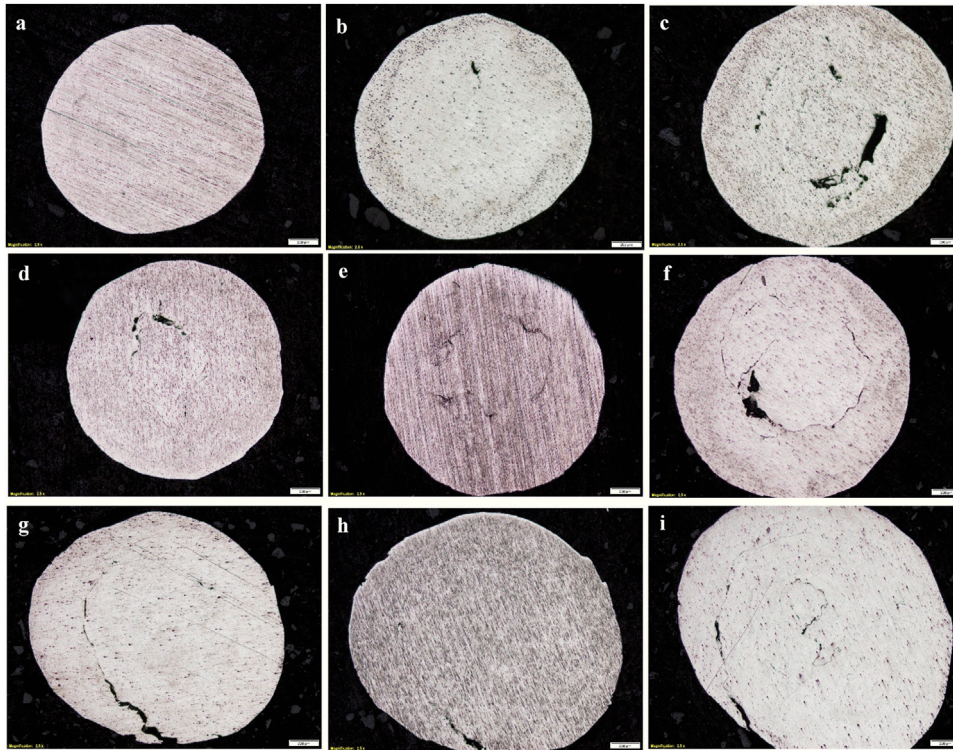


FIGURE 5 | (A-I) Optical microscopy images of three *in-situ* consolidated Al-Li-GNPs spheres milled for 8 h at several stages of polishing.

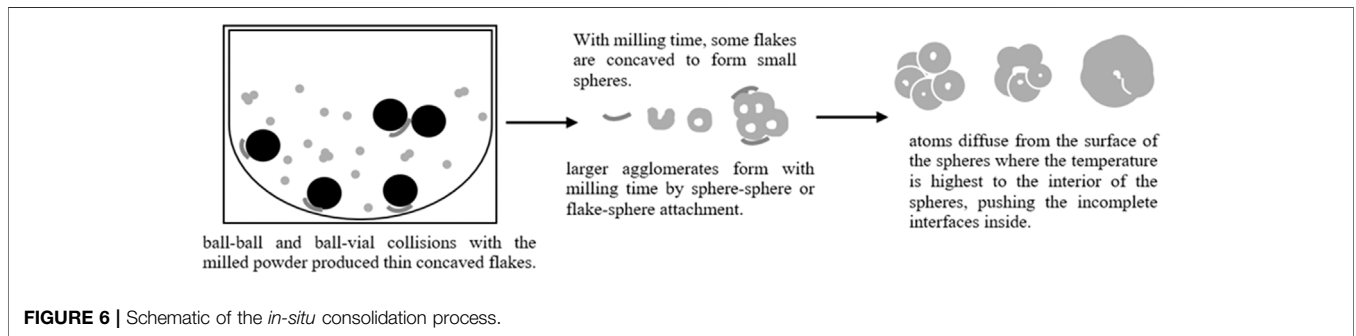
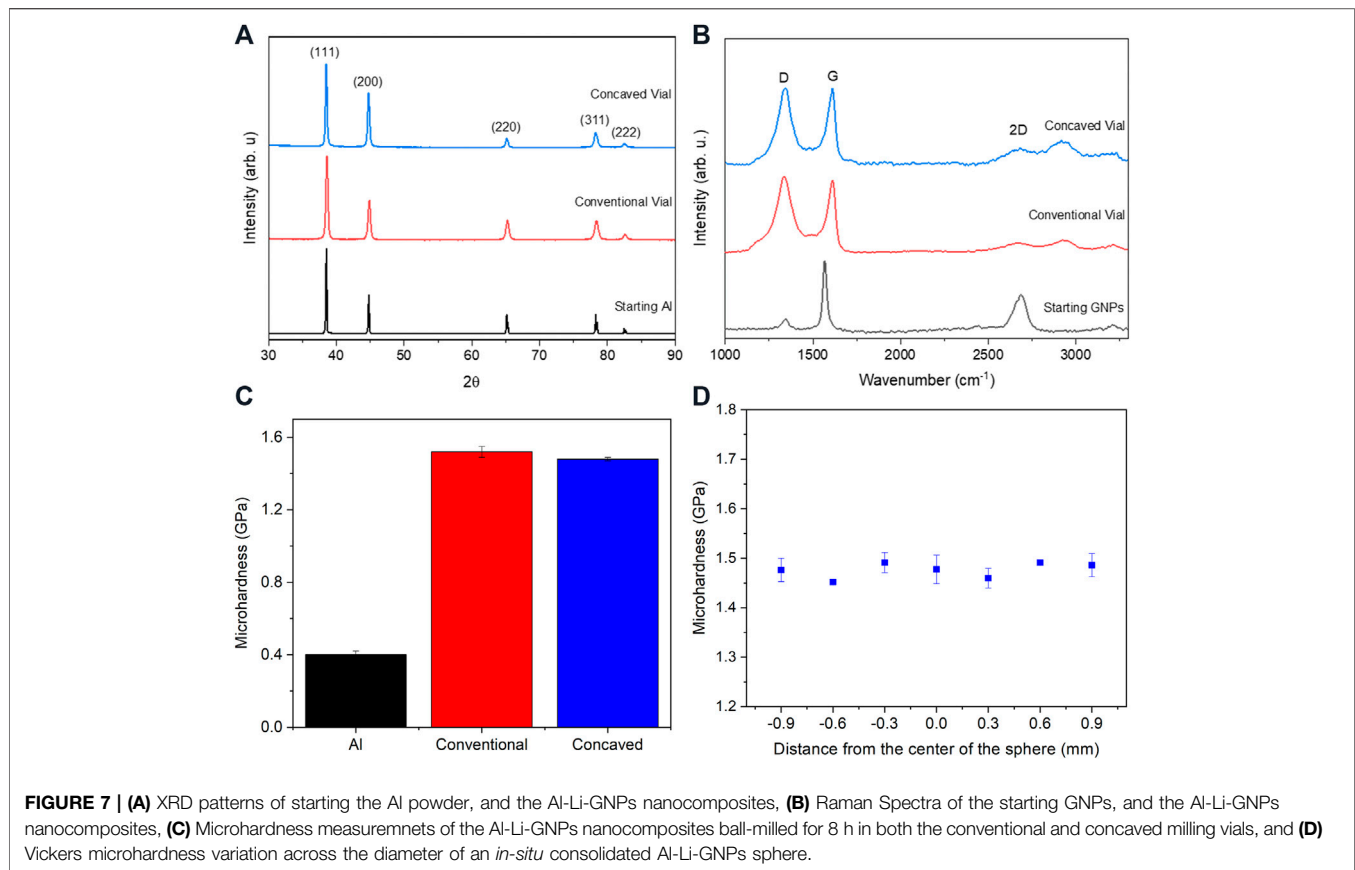


FIGURE 6 | Schematic of the *in-situ* consolidation process.

interfaces along with any other gaps in between them merge and result in the formation of elongated cracks near the surface. With continuous milling, the heat generated in the milling vial due to the repeated collisions will cause further bonding and diffusion to take place, and the atoms will diffuse from the surface of the sphere where the temperature is highest to the interior of the spheres, pushing the incomplete interface inside. This will continue until either the interface almost disappears or until the heat generated outside can no longer affect the diffusion of the interface, leaving smaller inner interfaces or voids in the middle of the sphere. Thus, it is expected that inducing a temperature rise during the last stages of milling can facilitate further diffusion and inter-particle bonding, thus help in achieving fully densified

spheres. A schematic of the consolidation steps is shown in **Figure 6**.

It is also interesting to note that Hegedús et al. (2017) investigated the effect of oxidation on the formation of *in-situ* consolidated spheres during ball-milling by milling in an inert argon atmosphere and in air. They concluded that unlike milling under argon, similar to our conditions, the presence of oxygen and impurities in the milled sample delayed or prevented the formation of *in-situ* consolidated spheres and resulted in the formation of flaky-like particles. Thus, they suggested that the presence of surface oxides hinders the cold welding of metals and that *in-situ* consolidation is an indication of the purity of the sample and a confirmation of the oxygen-free environment.



3.3 Crystal Structure, Grain Size, and Hardness

The effect of milling on the crystal structure, phase formation, and grain size of the Al-Li-GNPs ball-milled using both conventional and concaved milling vials was investigated by XRD, see **Figure 7A**. For comparison, the XRD pattern of the starting Al powder is included in **Figure 7** as well.

As indexed on the XRD patterns, the Al-Li-GNPs milled using both vials showed only a face-centered cubic (FCC) Al phase. No peaks were observed for the body-centered cubic (BCC) Li or any Al-Li second phases in the XRD pattern. This is attributed to the complete solubility of Li in Al, resulting in the formation of an FCC solid solution during ball-milling. The absence of any peaks for the GNPs could be attributed to the low content of GNPs (1.0 wt%) used (Bhadauria et al., 2019) and the lower scattering limit of C compared to metals (Bhadauria et al., 2019). In addition, no peaks were observed for Al_4C_3 , Al_2O_3 , or any second phases, indicating the minimal contamination of the prepared samples during milling. The formation of Al_4C_3 is highly investigated in GRAMC studies (Li et al., 2015; Zhang et al., 2016; Li and Xiong, 2017; Prashantha Kumar and Anthony Xavier, 2017). The formation of the brittle Al_4C_3 phase has been mainly attributed to the exposure to high temperatures during subsequent powder consolidation processes (Ahmad et al., 2020a), and was reported to be detrimental to the mechanical properties of GNPs/Al composites.

Grain size refinement and the introduction of lattice strain during the milling process can be interpreted by the XRD pattern with a larger broadening of the peaks [98]. As observed in **Figure 7**, the broadening of the peaks increased after milling for the Al-Li-GNPs samples as compared to the starting Al peaks. During the milling process, a substantial amount of energy is transferred from the milling balls to the powder being milled by the impact of collisions. This energy is stored in the milled powder in the form of severe plastic deformation occurring at high strain rates. This leads to the formation of high defect density including dislocations, vacancies, stacking faults, and a substantial increase in the grain boundary density (Mohammad Sharifi et al., 2012; Rane et al., 2013; Ebrahimi et al., 2019). The XRD line broadening was used to calculate the average grain size and lattice strain of nc Al using the integral breadth analysis and the Averbach formula (Klug and Alexander, 1974), see **Table 1**:

$$\frac{\beta^2}{\tan^2\theta_o} = \frac{\lambda}{d} \left(\frac{\beta}{\tan\theta_o \sin\theta_o} \right) + 25e^2 \quad (1)$$

Where β is the measured full-width half-maximum (FWHM) of the peak, θ_o is the peak's diffraction angle, λ is the x-ray wavelength of 0.154 nm, d is the average grain size, and e is the lattice strain. The grain size was calculated to be 38 and 48 nm, for the Al-Li-GNPs milled using the conventional and concaved milling vials, respectively. These values indicate successful grain refinement down to the nano regime (<100 nm) (Kumar

TABLE 1 | Properties of the ball-milled Al-Li-GNPs nanocomposites.

	Grain size (nm)	Lattice strain (%)	Microhardness (GPa)
Conventional Vial	38	0.16	1.52 ± 0.03
Concaved Vial	48	0.11	1.48 ± 0.02

et al., 2003; Attarilar et al., 2020), which is expected to significantly enhance the strength of the Al-based nanocomposite as predicted by the Hall–Petch relationship (Weertman, 1993).

The existence of the GNPs within the Al-Li matrix was first confirmed using Raman spectroscopy. In addition, Raman spectroscopy is generally used to investigate the effect of ball-milling on the structural integrity of the GNPs. The Raman spectra of the starting GNPs, and the Al-Li-GNPs nanocomposite milled using both milling vials can be seen in **Figure 7B**. The Raman spectra of all samples present the characteristic graphene peaks at around 1,350, 1,580, and 2,700 cm^{-1} , corresponding to the D, G, and 2D peaks, respectively (Ferrari et al., 2006). The introduction of structural defects in the GNPs after milling is inevitable due to the intensive nature of the high-energy ball-milling technique. The intensity ratio of the D-band to the G-band (I_D/I_G) is usually used to assess the degree of structural defects or disorders in sp^2 -based carbon structures and was found to increase from 0.14 for pure GNPs to 1.06 and 0.96 for the samples milled in the conventional and concaved milling vials, respectively. The lower I_D/I_G ratio measured for the *in-situ* consolidated Al-Li-GNPs is attributed to the formation of spheres and the material welding that took place early during milling, suggesting that the ductile Al matrix provided protection for the GNPs against the constant collision by the milling balls. This value is lower than the usually larger than 1.0 I_D/I_G ratios reported for ball-milled Al-Li-GNPs nanocomposites (Ahmad et al., 2020a). Another observation from **Figure 7B** is the positive shift and the broadening of the Raman bands. It has been reported that a shift in the peak position of the Raman bands is associated with residual stress accumulated in graphene (Aboukhair et al., 2019). This is because the interatomic distances in the graphene sheet change when graphene is strained, thus the vibration frequency changes and results in a wavenumber shift (Bastwros et al., 2014). Similar to the I_D/I_G ratio, the shift in the Raman bands confirm the introduction of defects and associated stresses during milling.

Vickers microhardness was used to investigate the mechanical properties of the ball-milled Al-Li-GNPs nanocomposite. To measure the hardness, the *in-situ* consolidated spheres milled in the concaved vial were polished into half, while the particles milled in the conventional milling vial were green pressed at 1 GPa into disks with 3 mm diameter and 1 mm thickness. The hardness of the Al-Li-GNPs *in-situ* consolidated spheres was measured to be 1.48 ± 0.02 GPa, slightly lower than the 1.52 ± 0.03 GPa measured for the Al-Li-GNPs sample milled in the conventional milling vial, see **Figure 7C**. The calculated grain size and measured microhardness values are expected

since *in-situ* consolidation of the entire sample did not occur in the conventional vial, suggesting that fracturing, and thus grain refinement, was still dominant over welding for longer milling times when the conventional milling vial was used. Nonetheless, significant strengthening is achieved as compared to the starting Al, for which the microhardness was measured to be 0.4 ± 0.02 GPa. For each hardness value reported in **Figures 7C, 8** hardness measurements were taken from different points for each sample, and no variation in hardness was observed (see insignificant error bars in **Figure 7C**). In addition, hardness measurements were taken across the diameter the polished surfaces of the *in-situ* consolidated sphere, see **Figure 7D**. The uniformity of the hardness measurements is an indication of the homogeneity of the as-milled microstructures in terms of a uniform grain size and GNPs distribution. Otherwise, microhardness measurements variation is an indication of a bimodal grain size microstructure or the agglomeration, and thus, the inhomogeneous distribution of the GNPs across the sample (Hu et al., 2018). This behavior was observed by Hu et al. (2018) in their GRAMC synthesized by ball-milling and 3D-printing. An increase in the error bars of the average hardness values was observed with increasing GNPs content. They attributed the scattered hardness values to the agglomeration of the graphene with larger GNPs additions. Thus, the uniformity of the hardness measurements throughout the cross-section as indicated by **Figure 7D**, confirms the uniformity of the prepared sample and the homogeneity of its microstructure, and thus the applicability of the consolidation technique for mechanical properties testing. The strengthening mechanisms in ball-milled GRAMCs have been attributed to grain refinement (Shin et al., 2015; Li and Xiong, 2017; Yue et al., 2017), load transfer between the GNPs reinforcement and the Al-based matrix (Pérez-Bustamante et al., 2014b; Shin et al., 2016; Li et al., 2018), the difference in the coefficient of thermal expansion (CTE) (Rashad et al., 2015b; Li and Xiong, 2017; Yue et al., 2017), and Orowan looping (Rashad et al., 2015c; Asgharzadeh and Sedigh, 2017; Yang et al., 2017).

The homogeneity of the *in-situ* consolidated Al-Li-GNPs nanocomposites was also confirmed by SEM-EDX mapping, see **Figure 8A**. The homogenous distribution of the GNPs within the *in-situ* consolidated Al-Li-GNPs sphere can be clearly indicated by the homogenous distribution of C as indicated by EDX in **Figure 8A**. Bright field TEM (BFTEM) images and the corresponding SAED patterns of the as milled Al-Li-GNPs milled using both conventional and concaved milling vials are shown in **Figures 8B,C**, respectively. The grains in all samples appear to be equiaxed with a random distribution within

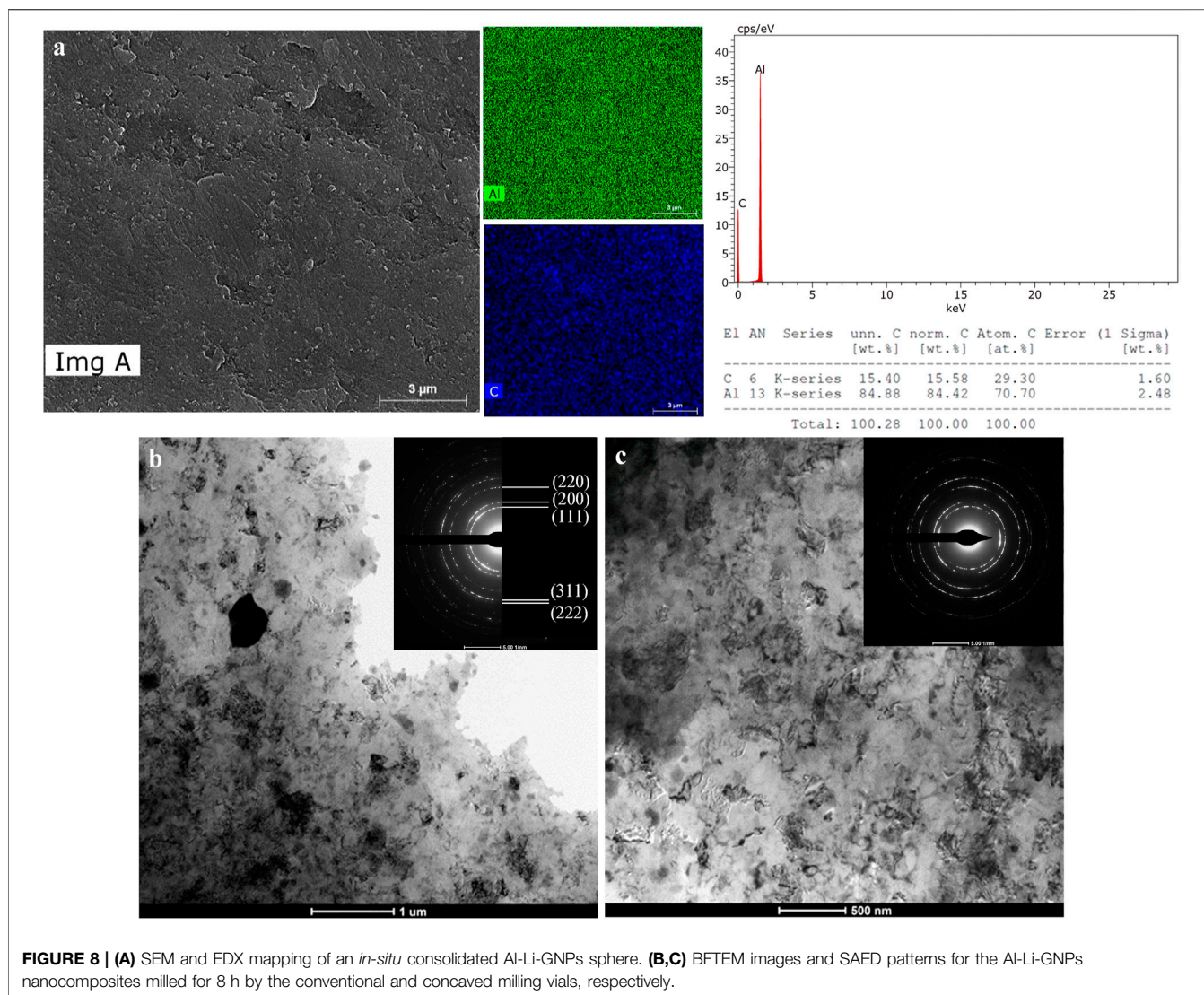


FIGURE 8 | (A) SEM and EDX mapping of an *in-situ* consolidated Al-Li-GNPs sphere. **(B,C)** BFTEM images and SAED patterns for the Al-Li-GNPs nanocomposites milled for 8 h by the conventional and concave milling vials, respectively.

the structure with no evidence for abnormal grains. In a concept similar to that of an XRD pattern, TEM SAED patterns give structural information and allow for secondary phase identification. In this regard, the indexed SAED ring patterns of the as-milled samples, see inset images in **Figure 8B**, confirm the XRD results of the presence of an FCC Al structure with nano grains and eliminates the presence of contamination from impurities, oxides, or the formation of second intermetallic phases. These results confirm the formation of the nanocrystalline Al-Li-GNPs nanocomposite within the *in-situ* consolidated spheres.

Thus far, studies have focused on the effect of temperature and/or process control agents on the *in-situ* consolidation of FCC milled powders (Zhang et al., 2002; Zhang et al., 2004; Youssef et al., 2006; Gupta et al., 2015; SamadiKhoshkhoo et al., 2015; Ahmad et al., 2020b). Broseghini et al. (2016) investigated the effect of the milling vial shape on the milling efficiency of high-energy planetary ball-mills. They redesigned the conventional

milling vial to have a flat side wall resulting in a half moon cross-section. Compared to the conventional cylindrical milling vial, the new geometry resulted in a larger number of high-velocity collisions, leading to a faster reduction of crystallite size compared to that using the standard cylindrical vial design. In a similar concept, the deformation of ductile particles due to the impact between the milling balls and the milled powder is affected by where the impact is taking place. By taking advantage of this information, a specially designed vial with a fully spherical interior was designed to initiate *in-situ* consolidation of ductile Al. Despite not achieving 100% densification, the results of this study prove that *in-situ* consolidation could be achieved without using a complicated 2-step cryomilling and room temperature ball-milling procedures. Instead, the results suggest that *in-situ* consolidation can occur at room temperature at much shorter times than in conventional milling vials by introducing another variable which was not previously considered in the ball-milling process: the shape of the milling vial. Introducing these

observations to the research community is the first step to further the investigations using different milling vials and different geometries to further investigate the *in-situ* consolidation possibilities and further enhance the powder densification. In addition, investigating the kinetics of ball impact in ball-milling vials with different geometries through modeling is required for an enhanced understanding of the observed phenomenon and for an efficient design of the optimized milling vial.

4 CONCLUSION

In this study, the possibility of achieving *in-situ* consolidation of a graphene reinforced Al-Li matrix composite using a simple room temperature ball-milling process was investigated by changing the shape of the conventionally used milling vial. For comparison, the ball-milling of Al-Li-1.0 wt% GNPs nanocomposite was conducted using both the conventional milling vial and a specially designed concaved milling vial. Results showed that the formation of *in-situ* consolidated uniform spheres with a nanometric grain size of 48 nm and high hardness of 1.48 ± 0.02 GPa was achieved after 8 h of milling using the concaved milling vial. Milling the same composition for 8 h in the conventional milling vial resulted in the formation of small particles with a grain size of 38 nm and a hardness of 1.52 ± 0.03 . Milling for longer hours in the conventional milling vial (up to 40 h) resulted in the formation of larger curved flakes and did not result in the *in-situ* consolidation of particles into spheres. Ball-milling has long been the most widely used lab technique for the synthesis of GRAMCs for mechanical properties testing, yet results have been hindered by the subsequent high temperature consolidation processes. The observations reported in this study shed light on a new possibility in the synthesis field of graphene-reinforced metal matrix

composites and is a step forward for achieving full densification of nanocrystalline materials synthesized by powder metallurgy techniques for reliable and reproducible mechanical strength testing.

DATA AVAILABILITY STATEMENT

The raw data supporting the conclusions of this article will be made available by the authors, without undue reservation.

AUTHOR CONTRIBUTIONS

SA: Conceptualization, Data curation, Formal analysis, Investigation, Methodology, Validation, Visualization, Writing—original draft. KY: Conceptualization, Investigation, Methodology, Funding acquisition, Project administration, Supervision, Writing—review and editing.

FUNDING

This research was funded by the Qatar National Research Fund (a member of the Qatar Foundation), grant number NPRP11S-1203-170056. The statements made herein are solely the responsibility of the authors.

ACKNOWLEDGMENTS

The authors would like to acknowledge the technical support provided by the Central Laboratory Unit and the Center of Advanced Materials at Qatar University, and the Qatar Environment and Energy Research Institute (QEERI).

REFERENCES

- Abaza, M. A., Al-Sulaiti, L., Scattergood, R. O., and Youssef, K. M. (2019). Influence of 1%Nb Solute Addition on the Thermal Stability of *In Situ* Consolidated Nanocrystalline Cu. *Adv. Eng. Mater.* 21, 1800859. doi:10.1002/adem.201800859
- Aboulkhair, N. T., Simonelli, M., Salama, E., Rance, G. A., Neate, N. C., Tuck, C. J., et al. (2019). Evolution of Carbon Nanotubes and Their Metallurgical Reactions in Al-Based Composites in Response to Laser Irradiation during Selective Laser Melting. *Mater. Sci. Eng. A* 765, 138307. doi:10.1016/j.msea.2019.138307
- Ahmad, S. I., Hamoudi, H., Abdala, A., Ghouri, Z. K., and Youssef, K. M. (2020). Graphene-Reinforced Bulk Metal Matrix Composites: Synthesis, Microstructure, and Properties. *Rev. Adv. Mater. Sci.* 59 (1), 67–114. doi:10.1515/rams-2020-0007
- Ahmad, S. I., Al-Sulaiti, L. A., Mkhoyan, K. A., and Youssef, K. M. (2020). Artifact-Free Bulk Nanocrystalline Al-Li Alloys with Multiple Deformation Mechanisms and Improved Tensile Properties. *Mater. Today Commun.* 25, 101607. doi:10.1016/j.mtcomm.2020.101607
- Ahmed, S. I., Mkhoyan, K. A., and Youssef, K. M. (2020). The Activation of Deformation Mechanisms for Improved Tensile Properties in Nanocrystalline Aluminum. *Mater. Sci. Eng. A* 777, 139069. doi:10.1016/j.msea.2020.139069
- Asgharzadeh, H., and Sedigh, M. (2017). Synthesis and Mechanical Properties of Al Matrix Composites Reinforced with Few-Layer Graphene and Graphene Oxide. *J. Alloys Compd.* 728, 47–62. doi:10.1016/j.jallcom.2017.08.268
- Ashwath, P., and Xavier, M. A. (2014). The Effect of Ball Milling & Reinforcement Percentage on Sintered Samples of Aluminium Alloy Metal Matrix Composites. *Proced. Eng.* 97, 1027–1032. doi:10.1016/j.proeng.2014.12.380
- Attarilar, S., Djavanroodi, F., Irfan, O. M., Al-Mufadi, F. A., Ebrahimi, M., and Wang, Q. D. (2020). Strain Uniformity Footprint on Mechanical Performance and Erosion-Corrosion Behavior of Equal Channel Angular Pressed Pure Titanium. *Results Phys.* 17, 103141. doi:10.1016/j.rinp.2020.103141
- Attarilar, S., Ebrahimi, M., Djavanroodi, F., Fu, Y., Wang, L., and Yang, J. (2021). 3D Printing Technologies in Metallic Implants: A Thematic Review on the Techniques and Procedures. *Int. J. Bioprint* 7 (1), 306. doi:10.18063/ijb.v7i1.306
- Attarilar, S., Djavanroodi, F., Ebrahimi, M., Al-Fadhalah, K. J., Wang, L., and Mozafari, M. (2021). Hierarchical Microstructure Tailoring of Pure Titanium for Enhancing Cellular Response at Tissue-Implant Interface. *J. Biomed. Nanotechnol.* 17 (1), 115–130. doi:10.1166/jbn.2021.3015
- Awotunde, M. A., Adegbenjo, A. O., Obadele, B. A., Okoro, M., Shongwe, B. M., and Olubambi, P. A. (2019). Influence of Sintering Methods on the Mechanical Properties of Aluminium Nanocomposites Reinforced with Carbonaceous Compounds: A Review. *J. Mater. Res. Technol.* 8 (2), 2432–2449. doi:10.1016/j.jmrt.2019.01.026

- Bastwros, M., Kim, G.-Y., Zhu, C., Zhang, K., Wang, S., Tang, X., et al. (2014). Effect of ball Milling on Graphene Reinforced Al6061 Composite Fabricated by Semi-solid Sintering. *Composites B: Eng.* 60, 111–118. doi:10.1016/j.compositesb.2013.12.043
- Bhadauria, A., Singh, L. K., and Laha, T. (2019). Combined Strengthening Effect of Nanocrystalline Matrix and Graphene Nanoplatelet Reinforcement on the Mechanical Properties of Spark Plasma Sintered Aluminum Based Nanocomposites. *Mater. Sci. Eng. A* 749, 14–26. doi:10.1016/j.msea.2019.02.007
- Bisht, A., Srivastava, M., Kumar, R. M., Lahiri, I., and Lahiri, D. (2017). Strengthening Mechanism in Graphene Nanoplatelets Reinforced Aluminum Composite Fabricated through Spark Plasma Sintering. *Mater. Sci. Eng. A* 695, 20–28. doi:10.1016/j.msea.2017.04.009
- Broseghini, M., D'Incau, M., Gelisio, L., Pugno, N. M., and Scardi, P. (2016). Effect of Jar Shape on High-Energy Planetary ball Milling Efficiency: Simulations and Experiments. *Mater. Des.* 110, 365–374. doi:10.1016/j.matdes.2016.06.118
- Chen, J. K., and Huang, I. S. (2013). Thermal Properties of Aluminum-Graphite Composites by Powder Metallurgy. *Composites Part B: Eng.* 44 (1), 698–703. doi:10.1016/j.compositesb.2012.01.083
- Chyada, F. A., Jabur, A. R., and Alwan, H. A. (2017). Effect Addition of Graphene on Electrical Conductivity and Tensile Strength for Recycled Electric Power Transmission Wires. *Energ. Proced.* 119, 121–130. doi:10.1016/j.egypro.2017.07.055
- Ebrahimi, M., Attarilar, S., Shaeri, M. H., Gode, C., Armoon, H., and Djavanroodi, F. (2019). An Investigation into the Effect of Alloying Elements on Corrosion Behavior of Severely Deformed Cu-Sn Alloys by Equal Channel Angular Pressing. *Arch. Civil Mech. Eng.* 19 (3), 842–850. doi:10.1016/j.acme.2019.03.009
- El-Danaf, E. A., Soliman, M. S., Almajid, A. A., and Khalil, K. A. (2013). Mechanical Characterization of Cryomilled Al Powder Consolidated by High-Frequency Induction Heat Sintering. *Adv. Mater. Sci. Eng.* 2013, 397351. doi:10.1155/2013/397351
- El-Ghazaly, A., Anis, G., and Salem, H. G. (2017). Effect of Graphene Addition on the Mechanical and Tribological Behavior of Nanostructured AA2124 Self-Lubricating Metal Matrix Composite. *Composites A: Appl. Sci. Manufacturing* 95, 325–336. doi:10.1016/j.compositesa.2017.02.006
- Ferrari, A. C., Meyer, J. C., Scardaci, V., Casiraghi, C., Lazzeri, M., Mauri, F., et al. (2006). Raman Spectrum of Graphene and Graphene Layers. *Phys. Rev. Lett.* 97 (18), 187401. doi:10.1103/PhysRevLett.97.187401
- Ghasali, E., Sangpour, P., Jam, A., Rajaei, H., Shirvanimoghaddam, K., and Ebadzadeh, T. (2018). Microwave and Spark Plasma Sintering of Carbon Nanotube and Graphene Reinforced Aluminum Matrix Composite. *Arch. Civil Mech. Eng.* 18 (4), 1042–1054. doi:10.1016/j.acme.2018.02.006
- Gupta, R. K., Fabijanic, D., Zhang, R., and Birbilis, N. (2015). Corrosion Behaviour and Hardness of In Situ Consolidated Nanostructured Al and Al-Cr Alloys Produced via High-Energy ball Milling. *Corrosion Sci.* 98, 643–650. doi:10.1016/j.corsci.2015.06.011
- Gürbüz, M., Can Şenel, M., and Koç, E. (2017). The Effect of Sintering Time, Temperature, and Graphene Addition on the Hardness and Microstructure of Aluminum Composites. *J. Compos. Mater.* 52 (4), 553–563. doi:10.1177/0021998317740200
- Hajjalilou, A., Kianvash, A., Lavvafi, H., and Shameli, K. (2018). Nanostructured Soft Magnetic Materials Synthesized via Mechanical Alloying: A Review. *J. Mater. Sci. Mater. Electron.* 29 (2), 1690–1717. doi:10.1007/s10854-017-8082-0
- Harris, A. M., Schaffer, G. B., and Page, N. W. (1993). The Russian Doll Effect by Mechanical Alloying. *J. Mater. Sci. Lett.* 12 (14), 1103–1104. doi:10.1007/bf00420534
- Hegedüs, Z., Meka, S. R., and Mittemeijer, E. J. (2017). In Situ Consolidation of Ball Milled Metals. *J. Alloys Compd.* 695, 721–725. doi:10.1016/j.jallcom.2016.11.035
- Hu, Z., Chen, F., Xu, J., Nian, Q., Lin, D., Chen, C., et al. (2018). 3D Printing Graphene-Aluminum Nanocomposites. *J. Alloys Compd.* 746, 269–276. doi:10.1016/j.jallcom.2018.02.272
- Huang, J. Y., Wu, Y. K., and Ye, H. Q. (1995). Ball Milling of Ductile Metals. *Mater. Sci. Eng. A* 199 (2), 165–172. doi:10.1016/0921-5093(94)09715-1
- Jiang, Y., Tan, Z., Xu, R., Fan, G., Xiong, D.-B., Guo, Q., et al. (2018). Tailoring the Structure and Mechanical Properties of Graphene Nanosheet/aluminum Composites by Flake Powder Metallurgy via Shift-Speed ball Milling. *Composites Part A: Appl. Sci. Manufacturing* 111, 73–82. doi:10.1016/j.compositesa.2018.05.022
- Klug, H. P., and Alexander, L. E. (1974). *X-Ray Diffraction Procedures: For Polycrystalline and Amorphous Materials*. 2nd Edition. New York, NY: Wiley, 992.
- Koch, C. C., Youssef, K. M., and Scattergood, R. O. (2008). Mechanical Properties of Nanocrystalline Materials Produced by In Situ Consolidation Ball Milling. *Mater. Sci. Forum* 579, 15–28. doi:10.4028/www.scientific.net/msf.579.15
- Kumar, K. S., Van Swygenhoven, H., and Suresh, S. (2003). Mechanical Behavior of Nanocrystalline Metals and alloys. *The Golden Jubilee Issue-Selected Topics in Materials Science and Engineering: Past, Present and Future*, Edited by S. Suresh. *Acta Materialia* 51 (19), 5743–5774. doi:10.1016/j.actamat.2003.08.032
- Kwon, H., Mondal, J., AlOgab, K. A., Sammelseg, V., Takamichi, M., Kawaski, A., et al. (2017). Graphene Oxide-Reinforced Aluminum alloy Matrix Composite Materials Fabricated by Powder Metallurgy. *J. Alloys Compd.* 698, 807–813. doi:10.1016/j.jallcom.2016.12.179
- Li, G., and Xiong, B. (2017). Effects of Graphene Content on Microstructures and Tensile Property of Graphene-Nanosheets/Aluminum Composites. *J. Alloys Compd.* 697, 31–36. doi:10.1016/j.jallcom.2016.12.147
- Li, J. L., Xiong, Y. C., Wang, X. D., Yan, S. J., Yang, C., He, W. W., et al. (2015). Microstructure and Tensile Properties of Bulk Nanostructured Aluminum/Graphene Composites Prepared via Cryomilling. *Mater. Sci. Eng. A* 626, 400–405. doi:10.1016/j.msea.2014.12.102
- Li, M., Gao, H., Liang, J., Gu, S., You, W., Shu, D., et al. (2018). Microstructure Evolution and Properties of Graphene Nanoplatelets Reinforced Aluminum Matrix Composites. *Mater. Characterization* 140, 172–178. doi:10.1016/j.matchar.2018.04.007
- Li, W., Yang, X., He, C., Sha, J., Shi, C., Li, J., et al. (2019). Compressive Responses and Strengthening Mechanisms of Aluminum Composite Foams Reinforced with Graphene Nanosheets. *Carbon* 153, 396–406. doi:10.1016/j.carbon.2019.07.043
- Meyers, M. A., and Taylor Aimone, C. (1983). Dynamic Fracture (Spalling) of Metals. *Prog. Mater. Sci.* 28 (1), 1–96. doi:10.1016/0079-6425(83)90003-8
- Mohammad Sharifi, E., Enayati, M. H., and Karimzadeh, F. (2012). Fabrication and Characterization of Al-Al4c3 Nanocomposite by Mechanical Alloying. *Int. J. Mod. Phys. Conf. Ser.* 05, 480–487. doi:10.1142/s2010194512002371
- Najimi, A. A., and Shahverdi, H. R. (2017). Effect of Milling Methods on Microstructures and Mechanical Properties of Al6061-CNT Composite Fabricated by Spark Plasma Sintering. *Mater. Sci. Eng. A* 702, 87–95. doi:10.1016/j.msea.2017.04.041
- Pérez-Bustamante, R., Bolaños-Morales, D., Bonilla-Martínez, J., Estrada-Guel, I., and Martínez-Sánchez, R. (2014). Microstructural and Hardness Behavior of Graphene-Nanoplatelets/aluminum Composites Synthesized by Mechanical Alloying. *J. Alloys Compd.* 615, S578–S582. doi:10.1016/j.jallcom.2014.01.225
- Pérez-Bustamante, R., Bolaños-Morales, D., Bonilla-Martínez, J., Estrada-Guel, I., and Martínez-Sánchez, R. (2014). Microstructural and Hardness Behavior of Graphene-Nanoplatelets/aluminum Composites Synthesized by Mechanical Alloying. *J. Alloys Compd.* 615 (Suppl. 1), S578–S582. doi:10.1016/j.jallcom.2014.01.225
- Pradhan, S. K., Sahoo, M. R., Ratha, S., Polai, B., Mitra, A., Sathpathy, B., et al. (2020). Graphene-incorporated Aluminum with Enhanced thermal and Mechanical Properties for Solar Heat Collectors. *AIP Adv.* 10 (6), 065016. doi:10.1063/5.0008786
- Prashantha Kumar, H. G., and Anthony Xavier, M. (2017). Processing and Characterization of Al 6061 - Graphene Nanocomposites. *Mater. Today Proc.* 4 (2), 3308–3314. doi:10.1016/j.matpr.2017.02.217
- Rajkumar, K., and Aravindan, S. (2009). Microwave Sintering of Copper-Graphite Composites. *J. Mater. Process. Technol.* 209 (15), 5601–5605. doi:10.1016/j.jmatprot.2009.05.017
- Ram Prakash, S., Selvakumar, G., and Rajkumar, K. (2021). Spark Plasma Processing of Semi-conductive Titanium Carbide Dispersed Alumina Composites. *Mater. Manufacturing Process.* 37, 81–89. doi:10.1080/10426914.2021.1944196
- Rane, G. K., Welzel, U., Meka, S. R., and Mittemeijer, E. J. (2013). Non-Monotonic Lattice Parameter Variation with Crystallite Size in Nanocrystalline Solids. *Acta Materialia* 61 (12), 4524–4533. doi:10.1016/j.actamat.2013.04.021

- Rashad, M., Pan, F., Zhang, J., and Asif, M. (2015). Use of High Energy Ball Milling to Study the Role of Graphene Nanoplatelets and Carbon Nanotubes Reinforced Magnesium Alloy. *J. Alloys Compd.* 646, 223–232. doi:10.1016/j.jallcom.2015.06.051
- Rashad, M., Pan, F., Hu, H., Asif, M., Hussain, S., and She, J. (2015). Enhanced Tensile Properties of Magnesium Composites Reinforced with Graphene Nanoplatelets. *Mater. Sci. Eng. A* 630, 36–44. doi:10.1016/j.msea.2015.02.002
- Rashad, M., Pan, F., Tang, A., Asif, M., Hussain, S., Gou, J., et al. (2015). Improved Strength and Ductility of Magnesium with Addition of Aluminum and Graphene Nanoplatelets (Al+GNPs) Using Semi Powder Metallurgy Method. *J. Ind. Eng. Chem.* 23, 243–250. doi:10.1016/j.jiec.2014.08.024
- Saheb, N. (2013). Spark Plasma and Microwave Sintering of Al6061 and Al2124 Alloys. *Int. J. Miner Metall. Mater.* 20 (2), 152–159. doi:10.1007/s12613-013-0707-6
- Sakher, E., Loudjani, N., Benchiheb, M., and Bououdina, M. (2018). Influence of Milling Time on Structural and Microstructural Parameters of Ni50Ti50 Prepared by Mechanical Alloying Using Rietveld Analysis. *J. Nanomater.* 2018, 2560641. doi:10.1155/2018/2560641
- Samadi Khoshkhoo, M., Scudino, S., Gemming, T., Thomas, J., Freudenberger, J., Zehetbauer, M., et al. (2015). Nanostructure Formation Mechanism during In-Situ Consolidation of Copper by Room-Temperature ball Milling. *Mater. Des. (1980-2015)* 65, 1083–1090. doi:10.1016/j.matdes.2014.06.052
- Shin, S. E., and Bae, D. H. (2015). Deformation Behavior of Aluminum Alloy Matrix Composites Reinforced with Few-Layer Graphene. *Composites Part A: Appl. Sci. Manufacturing* 78, 42–47. doi:10.1016/j.compositesa.2015.08.001
- Shin, S. E., Choi, H. J., Shin, J. H., and Bae, D. H. (2015). Strengthening Behavior of Few-Layered Graphene/Aluminum Composites. *Carbon* 82, 143–151. doi:10.1016/j.carbon.2014.10.044
- Shin, S. E., Ko, Y. J., and Bae, D. H. (2016). Mechanical and Thermal Properties of Nanocarbon-Reinforced Aluminum Matrix Composites at Elevated Temperatures. *Composites Part B: Eng.* 106, 66–73. doi:10.1016/j.compositesb.2016.09.017
- Suryanarayana, C. (2019). Mechanical Alloying: A Novel Technique to Synthesize Advanced Materials. *Research* 2019, 4219812. doi:10.34133/2019/4219812
- Tabandeh-Khorshid, M., Omrani, E., Menezes, P. L., and Rohatgi, P. K. (2016). Tribological Performance of Self-Lubricating Aluminum Matrix Nanocomposites: Role of Graphene Nanoplatelets. *Eng. Sci. Technol. Int. J.* 19 (1), 463–469. doi:10.1016/j.jestch.2015.09.005
- Tiwari, J. K., Mandal, A., Rudra, A., Sathish, N., Kumar, S., and Singh, A. K. (2020). Influence of Graphene Content on the Mechanical Properties of Severely Deformed Graphene/Aluminum Composite. *Mater. Chem. Phys.* 248, 122939. doi:10.1016/j.matchemphys.2020.122939
- Toozandehjani, M., Matori, K., Ostovan, F., Abdul Aziz, S., and Mamat, M. (2017). Effect of Milling Time on the Microstructure, Physical and Mechanical Properties of Al-Al₂O₃ Nanocomposite Synthesized by Ball Milling and Powder Metallurgy. *Materials* 10 (11), 1232. doi:10.3390/ma10111232
- Wang, J., Guo, L.-N., Lin, W.-M., Chen, J., Liu, C.-L., Chen, S.-D., et al. (2019). Effect of the Graphene Content on the Microstructures and Properties of Graphene/Aluminum Composites. *New Carbon Mater.* 34 (3), 275–285. doi:10.1016/s1872-5805(19)60016-8
- Weertman, J. R. (1993). Hall-Petch Strengthening in Nanocrystalline Metals. *Mater. Sci. Eng. A* 166, 161–167. doi:10.1016/0921-5093(93)90319-a
- Wu, Z. M., Liang, Y. X., Fan, Y., Wang, P. P., Du, J. L., Zhao, Y. B., et al. (2018). The ball to Powder Ratio (BPR) Dependent Morphology and Microstructure of Tungsten Powder Refined by ball Milling. *Powder Technol.* 339, 256–263. doi:10.1016/j.powtec.2018.07.094
- Yang, M., Weng, L., Zhu, H., Fan, T., and Zhang, D. (2017). Simultaneously Enhancing the Strength, Ductility and Conductivity of Copper Matrix Composites with Graphene Nanoribbons. *Carbon* 118, 250–260. doi:10.1016/j.carbon.2017.03.055
- Youssef, K. M., Scattergood, R. O., Linga Murty, K., and Koch, C. C. (2004). Ultratough Nanocrystalline Copper with a Narrow Grain Size Distribution. *Appl. Phys. Lett.* 85 (6), 929–931. doi:10.1063/1.1779342
- Youssef, K. M., Scattergood, R. O., Murty, K. L., and Koch, C. C. (2006). Nanocrystalline Al-Mg Alloy with Ultrahigh Strength and Good Ductility. *Scripta Materialia* 54 (2), 251–256. doi:10.1016/j.scriptamat.2005.09.028
- Yu, Z., Yang, W., Zhou, C., Zhang, N., Chao, Z., Liu, H., et al. (2019). Effect of Ball Milling Time on Graphene Nanosheets Reinforced Al6063 Composite Fabricated by Pressure Infiltration Method. *Carbon* 141, 25–39. doi:10.1016/j.carbon.2018.09.041
- Yue, H., Yao, L., Gao, X., Zhang, S., Guo, E., Zhang, H., et al. (2017). Effect of Ball-Milling and Graphene Contents on the Mechanical Properties and Fracture Mechanisms of Graphene Nanosheets Reinforced Copper Matrix Composites. *J. Alloys Compd.* 691, 755–762. doi:10.1016/j.jallcom.2016.08.303
- Zhang, X., Wang, H., Kassem, M., Narayan, J., and Koch, C. C. (2002). Preparation of Bulk Ultrafine-Grained and Nanostructured Zn, Al and Their Alloys by In Situ Consolidation of Powders during Mechanical Attrition. *Scripta Materialia* 46 (9), 661–665. doi:10.1016/s1359-6462(02)00048-9
- Zhang, X., Wang, H., and Koch, C. C. (2004). Mechanical Behavior of Bulk Ultrafine-Grained and Nanocrystalline Zn. *Rev. Adv. Mater. Sci.* 6 (2), 53–93.
- Zhang, H., Xu, C., Xiao, W., Ameyama, K., and Ma, C. (2016). Enhanced Mechanical Properties of Al5083 Alloy with Graphene Nanoplates Prepared by ball Milling and Hot Extrusion. *Mater. Sci. Eng. A* 658, 8–15. doi:10.1016/j.msea.2016.01.076
- Zhao, K. Y., Li, C. J., Tao, J. M., Ng, D. H. L., and Zhu, X. K. (2010). The Synthesis, Microstructure, Hardness and Thermal Properties of Bulk Nanocrystalline Al Produced by In Situ Consolidation with Low-Energy Ball Milling. *J. Alloys Compd.* 504, S306–S310. doi:10.1016/j.jallcom.2010.03.204
- Zhu, X. K., Zhang, X., Wang, H., Sergueeva, A. V., Mukherjee, A. K., Scattergood, R. O., et al. (2003). Synthesis of Bulk Nanostructured Zn by Combinations of Cryomilling and Powder Consolidation by Room Temperature Milling: Optimizing Mechanical Properties. *Scripta materialia* 49 (5), 429–433. doi:10.1016/s1359-6462(03)00297-5

Conflict of Interest: The authors declare that the research was conducted in the absence of any commercial or financial relationships that could be construed as a potential conflict of interest.

Publisher's Note: All claims expressed in this article are solely those of the authors and do not necessarily represent those of their affiliated organizations, or those of the publisher, the editors and the reviewers. Any product that may be evaluated in this article, or claim that may be made by its manufacturer, is not guaranteed or endorsed by the publisher.

Copyright © 2022 Ahmad and Youssef. This is an open-access article distributed under the terms of the Creative Commons Attribution License (CC BY). The use, distribution or reproduction in other forums is permitted, provided the original author(s) and the copyright owner(s) are credited and that the original publication in this journal is cited, in accordance with accepted academic practice. No use, distribution or reproduction is permitted which does not comply with these terms.